Application of Cairns-Tsallis distribution to the dipole-type Hamiltonian mean-field model

Ewin Sánchez [*]

*Instituto de Investigación Multidisciplinario en Ciencia y Tecnología, Universidad de La Serena, La Serena 170000, Chile
and Departamento de Física, Universidad de La Serena, Avenida Juan Cisternas 1200, La Serena 170000, Chile*

Boris Atenas [†]

Departamento de Física, Facultad de Ciencias, Universidad de Tarapacá, Casilla 7-D, Arica, Chile

We found that the rare distribution of velocities in quasisteady states of the dipole-type Hamiltonian mean-field model can be explained by the Cairns-Tsallis distribution, which has been used to describe nonthermal electron populations of some plasmas. This distribution gives us two interesting parameters which allow an adequate interpretation of the output data obtained through molecular dynamics simulations, namely, the characteristic parameter q of the so-called nonextensive systems and the α parameter, which can be seen as an indicator of the number of particles with nonequilibrium behavior in the distribution. Our analysis shows that fit parameters obtained for the dipole-type Hamiltonian mean-field simulated system are *ad hoc* with some nonthermality and nonextensivity constraints found by different authors for plasma systems described through the Cairns-Tsallis distribution.

I. INTRODUCTION

Since the emergence of statistical mechanics and kinetic theory, we have been able to study systems composed of a large number of constituent elements using the statistical description of macroscopic observable quantities related to thermodynamics from the classical microscopic study (first principles), i.e., the knowledge of the positions and velocities of particles that form the system (Hamiltonian and initial conditions), or equivalently the knowledge of probabilities [microcanonical ensemble with equiprobable states, canonical ensemble (i.e., states with a canonical probability associated with the thermal reservoir), etc.]. The success of this description is widely known in the early works of Einstein on the specific heat of a solid and the Brownian motion. Since then, various theoretical models (Debye, Ising, Drude, Heisenberg, etc.) have been proposed to try to capture natural phenomena present in materials, such as phase transitions. Although the assumptions made in theoretical models are often absurd or grotesque, these considerations end up capturing part of the reality observed in nature, such as the two-dimensional (2D) Ising model, which exhibits a paramagnetic-ferromagnetic-type phase transition. Over time, improvements were made to this model, such as the Heisenberg model. However, the interactions present in the systems are often largely combinations of short- and long-range interactions. When long-range interactions are considered, conventional statistical mechanics fails since several of the considerations that define equilibrium and probability distributions rely on a property known as

additivity, which is not satisfied in long-range systems. This property is associated with macroscopic quantities such as energy or entropy. If the energy (entropy) of a system is additive, it can be separated into the sum of the energies (entropies) of the subsystems, $U_T = U_A + U_B$, $S(U_T) = S(U_A) + S(U_B)$. This allows the establishment of equilibrium conditions widely known as the equalization of inverse temperatures $\beta_I = \beta_{II}$, pressures $p_I = p_{II}$, or chemical potentials $\mu_I = \mu_{II}$. When this property fails, there is a possibility that another property known as extensivity [namely, the property that the energy (entropy) of the system scales proportionally to the number of particles] can be recovered through a Kac's prescription (in terms of theoretical models). When extensivity is satisfied, we can recover the entire Duhem-Gibbs structure of the Legendre transforms and guarantee the correct description of thermodynamics. In the pursuit of a statistical explanation for the behavior of complex or long-range interacting nonequilibrium systems, various formalisms have been proposed to elucidate the non-Boltzmannian behavior. These formalisms include the kappa distribution [1], the Lynden-Bell formalism [2], the Tsallis formalism [3], superstatistics [4], and the maximum caliber formalism [5], among others. It is noteworthy that these approaches have sparked discussions and diverse perspectives among researchers [6–8]. Such formalisms have contributed to building a framework of nonequilibrium statistical mechanics. In this paper we focus on the description of a kind of quasistationary state involved in the nonequilibrium dynamics that previously it had not been possible to describe by means of the Tsallis distribution, Lynden-Bell statistics, or Tsallis-like Vlasov solutions [6,9,10]. This paper is organized as follows. In Sec. II we present the dipole-type Hamiltonian mean-field (d-HMF) model that is used to study the quasistationary states (QSSs)

---
[*]esanchez@userena.cl
[†]batenas@academicos.uta.cl

present in nonequilibrium dynamics. Section III presents the Cairns-Tsallis distribution (CTD) used to describe the QSSs present in the d-HMF model. In Sec. IV we present the results obtained.

II. THE d-HMF MODEL

This study focuses on a specific kind of nonequilibrium system known as the d-HMF model, which was recently introduced by Atenas and Curilef [11] and Atenas [12]. The d-HMF is a classical Hamiltonian mean-field model (zero order) inspired by electric dipolar interactions [11,13–15]. The system under consideration comprises a collection of classical rotors with long-range interactions. This nonsymmetric model exhibits a second-order phase transition.

The Hamiltonian of the d-HMF is given by

$$H = \sum_{i=1}^{N} \frac{p_i^2}{2} + \frac{\lambda}{2N} \sum_{i\neq j}^{N} (\cos(\theta_i - \theta_j) - 3\cos\theta_i \cos\theta_j + 2),$$
(1)

where the mass of each particle is equal to 1, p_i is the momentum, and θ_i is the orientation of the dipole i. N is the number of dipoles and λ is the coupling, which is ferromagnetic when λ is positive and antiferromagnetic when it is negative. The equations of motion and the potential energy V of the system can be expressed in terms of magnetization components,

$$\vec{M} = (m_x, m_y) = \frac{1}{N} \sum_i (\cos\theta_i, \sin\theta_i);$$
(2)

then,

$$\dot{p}_i = -\lambda(2m_x \sin\theta_i + m_y \cos\theta_i),$$
(3)

$$V = \frac{\lambda N}{2} (2 - 2m_x^2 + m_y^2).$$
(4)

In the thermodynamic limit, whether by counting states in the microcanonical ensemble or by computing the partition function in the canonical ensemble, both approaches result in the equilibrium solution,

$$\varepsilon = \frac{1}{2\beta} + 1 - m^2,$$
(5)

where m is the modulus of the magnetization, and it is the solution of the equation

$$x = \frac{I_1(2\beta\lambda x)}{I_0(2\beta\lambda x)},$$
(6)

where I_1 and I_0 are modified Bessel functions of the first kind.

In nonequilibrium, the system is characterized by the presence of two distinct quasistationary states (QSS-1 and QSS-2) involved in the dynamics leading to equilibrium (see Fig. 1). Notably, these states of apparent equilibrium are characterized by the system's maintenance of constant average kinetic energy for a significant duration. Those states are observed when uniform distributions (water-bag) initial conditions are used in molecular dynamics simulations [11,13,16,17]. Additionally, this type of quasiequilibrium is marked by the occurrence of negative specific heat. Previous studies [11,13–15] have
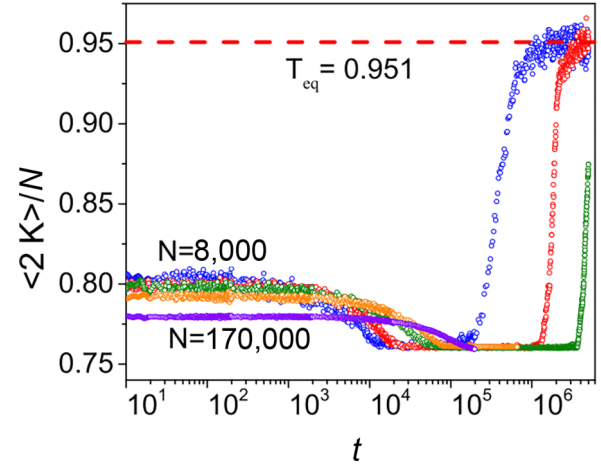

FIG. 1. Quasistationary states involved in the d-HMF model. Average kinetic energy per particle as a function of time for different numbers of particles, $N = 8000$, $N = 16\,000$, $N = 32\,000$, $N = 70\,000$, and $N = 170\,000$; data were obtained from molecular dynamics simulations.

revealed anomalous diffusion regimes and established a scaling law for the lifetime of QSSs.

Figure 2 shows the shapes of the first and second QSSs and equilibrium. Figures 2(a) and 2(b) are from QSS-1, Fig. 2(c) is from QSS-2, and Fig. 2(d) is from equilibrium. It can be observed that the distribution of orientations during QSS-2 is relatively constant (uniform), which is consistent with the fact that the magnetization during the QSS-2 is near zero, which responds to an equilibrium of forces from Eq. (2), where m_y is also near zero. In contrast, QSS-1 is highly dependent on the initial conditions; it is observed that the distribution of orientations continues to be highly localized. This fact was also observed in Ref. [18]. Figure 3 is a result of previous work [15]. It depicts the peculiar momentum distribution of
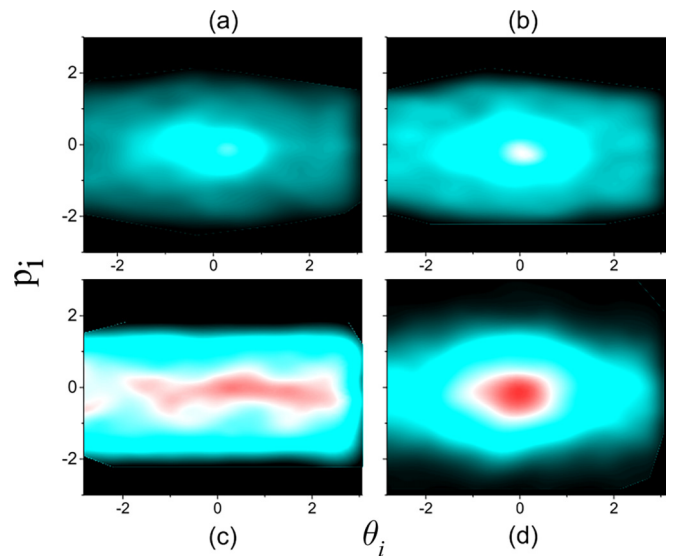

FIG. 2. System phase space snapshots obtained with molecular dynamics data outputs: (a) and (b) QSS-1, (c) QSS-2, and (d) equilibrium.
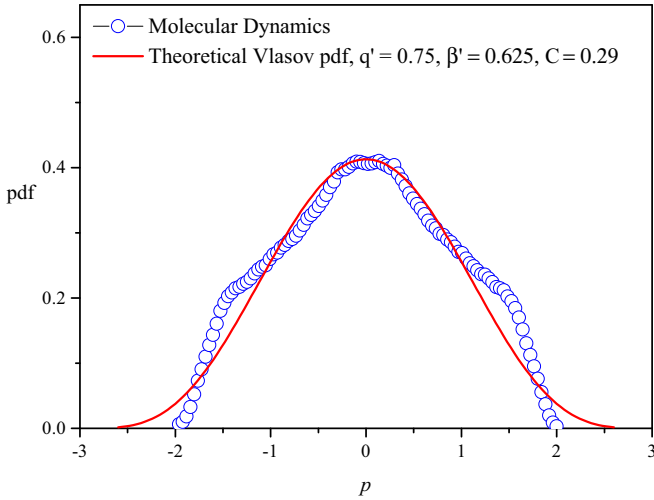
FIG. 3. Momentum distribution of the d-HMF model and a Tsallis-Like Vlasov pdf.

QSS-1, where blue circles correspond to molecular dynamics simulations and the red curve is a Tsallis-like Vlasov solution given by

$$f(\theta, p) = C(1 - (1 - q')\beta' e(\theta, p))^{\frac{1}{1-q'}}, \qquad (7)$$

where C is a normalization constant, q' and β' are parameters, and $e(\theta, p)$ is the individual particle energy. It is well known that stationary solutions must be functions of the individual energy. In the mentioned paper [15] it was found that is not possible to describe QSS-1 by a Tsallis-like Vlasov solution or by a Tsallis distribution. This fact motivated the search for an alternative distribution in this paper to describe these states adequately. Such a distribution is the Cairns-Tsallis distribution, as will be seen below.

III. THE CAIRNS-TSALLIS DISTRIBUTION

A. Background

An ideal plasma can be viewed as a classical system in thermal equilibrium, where particles show a zero correlation with a characteristic Maxwellian distribution (MD) of velocities. On the other hand, we have a nonthermal plasma, which is not in thermodynamic equilibrium and shows a velocity distribution compatible with non-Maxwellian superthermal distributions, such as the Vasyliunas distribution (VD). This distribution, also known as the kappa distribution, is given by

$$p(x) = \frac{n}{\theta_\kappa(\pi\kappa)^{1/2}} \frac{\Gamma(\kappa + 1)}{\Gamma(\kappa - 1/2)} \left(1 + \frac{v^2}{\kappa\theta_\kappa^2}\right)^{-\kappa}, \qquad (8)$$

here in the one-dimensional representation (as can be seen in Ref. [19]), where n is the particle number density and $\theta_\kappa = [(2\kappa - 3)/\kappa]^{1/2}(T/m)^{1/2}$ is the thermal velocity, with T being the particle temperature. The VD function was proposed in Ref. [1] to investigate the population of low-energy electrons in the satellite-observed magnetosphere. The spectral index κ accounts for the observed superthermal particles. When κ decreases, we have more superthermal particles in the tail of the distribution function, and when $\kappa \to \infty$, we have the system

in a thermal equilibrium, with velocities described by a MD function. With the VD function, many naturally occurring and artificial plasmas have been described, and its connection with the Tsallis nonextensive statistical mechanics was established later. In-depth analysis of the relationship between the nonextensive q-exponential and VD functions has been provided in several papers, such as in Refs. [20–22]. In those papers we can verify that for the VD function, given by Eq. (8), transformation $\kappa = 1/(q - 1)$ provides us the nonextensive Tsallis distribution (TD)

$$p_q(v) \propto \left[1 + (q - 1)\frac{v^2}{\theta_q^2}\right]^{-\frac{1}{q-1}}. \qquad (9)$$

When $q \to 1$, we have the thermal Maxwellian distribution.

On the other hand, there is another known function to describe populations of high-energy particles. We also have the (one-dimensional) Cairns distribution (CD), which showed that nonthermal distribution of electrons has an impact on ion sound solitary structures [23]. It is given by

$$p(x) = \frac{n}{(3\alpha + 1)\sqrt{2\pi\theta^2}}\left(1 + \frac{\alpha v^4}{\theta^4}\right)\exp\left(-\frac{v^2}{2\theta^2}\right). \qquad (10)$$

$\theta = (T/m)^{1/2}$, and α is the nonthermality parameter, which is a measure of the deviation from a Maxwellian distribution. A value of $\alpha = 0$ corresponds to the MD function, while a value of $\alpha > 0$ corresponds to a non-Maxwellian distribution with a heavier tail, which suggests that electrons are not in thermal equilibrium with the surrounding plasma. The nonthermality parameter can also be used to study the effects of nonthermal particles on plasma waves.

Other new proposals have emerged more recently. These include the skew-kappa model [24] and the generalized (r, q) distribution [25], among others. However, we will place our attention on Ref. [26], where a nonextensive nonthermal velocity distribution was presented. This is the Cairns-Tsallis distribution (CTD) given by

$$p(x) \propto \left(1 + \frac{\alpha v^4}{\theta^4}\right)\left[1 + (q - 1)\frac{v^2}{\theta_q^2}\right]^{-\frac{1}{q-1}}. \qquad (11)$$

From this, we have the TD function for $\alpha = 0$, the CD function for $q \to 1$, and the MD function for $\alpha = 0$ and $q \to 1$ simultaneously. Many authors have applied this function, showing that a superadditive regime ($q < 1$) can describe some nonthermal plasmas. This class of Tsallis velocity distribution with nonextensive q parameter smaller than unity has already been analyzed and commented upon by different plasma researchers [27–29]. The great flexibility of this function can be seen in Fig. 4 when $\alpha = 0.50$ and q takes different values. For other values of α and q, significant effects can be observed in the shoulder and/or the tail of the distribution curve. Because of this, the CTD function can be fitted to data distributions with unusual appearances on the respective plots, unattainable by many proposed models in the literature. This function has been extensively studied by other authors, performing linear and nonlinear analysis to see the effect on electron-acoustic wave propagation [30–33] as well as the effect of the dust grain charging process in a non-Maxwellian dusty plasma [34,35].
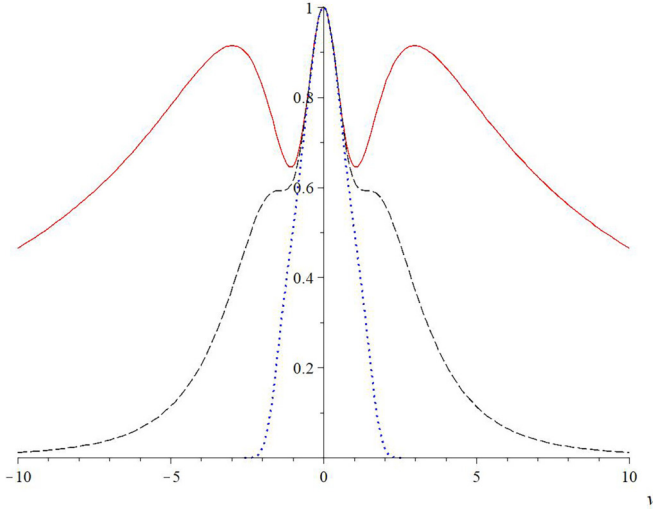
FIG. 4. The Cairns-Tsallis distribution. Fit curves for $\alpha = 0.50$ and $q = 1.40$ (solid red curve), $q = 1.25$ (dashed black curve), and $q = 0.85$ (dotted blue curve).

B. Superstatistical framework

Let us present a brief summary of the superstatistics theory presented in Ref. [4] and then show that the CD and TD functions can arise from it. It is a generalization of the nonextensive statistical mechanics based on the superposition of two different statistics prevailing in a driven nonequilibrium system with a stationary state. Superstatistics is compatible with systems characterized by a superposition of several dynamics on separated time scales. The corresponding evolution is characterized by spatiotemporal fluctuations of an intensive parameter β, according to the probability density $g(\beta)$. From this, a more general statistics arises to describe the energy E distribution of those systems, namely, the superstatistical distribution

$$p(E) = \int e^{-\beta E} g(\beta) d\beta, \tag{12}$$

which is seen as a generalized Boltzmann factor. It can be written as $B(E) = \langle e^{-\beta E} \rangle$, with $\beta \equiv 1/T$. A long list of papers dealing with plasma systems through the superstatistical perspective can be found in the most recent literature, such as Refs. [36–39]. However, we will focus on Ref. [40], since results in that paper are intimately connected with the CTD function, as will be seen below. So far we have not found a function $g(\beta)$ such that the integral (12) provides the CTD function as a solution; however, it is possible to obtain each of the factors that compose it, that is, the TD and CD functions. In this way we could interpret both distributions as a consequence of temperature fluctuations, as suggested in the mentioned paper [40]. For the one-dimensional case, the above can arise from (12): Taking a Maxwellian distribution $f(v|\beta)$ instead of the Boltzmann distribution, with

$$f(v|\beta) = \sqrt{\frac{\beta}{2\pi}} e^{-\frac{\beta v^2}{2}} \tag{13}$$

and assuming that β is χ^2 distributed

$$g(\beta) = \left(\frac{n}{2\beta_0}\right)^{\frac{n}{2}} \frac{\beta^{n/2-1}}{\Gamma(n/2)} e^{-\frac{n\beta}{2\beta_0}}, \tag{14}$$

we obtain that the un-normalized Eq. (12) is

$$p(v) = \left(1 + \frac{\beta_0}{n} v^2\right)^{-\frac{n}{2} - \frac{1}{2}}. \tag{15}$$

We can readily see that TD function of the nonextensive statistical mechanics appears when $n = \frac{2}{q-1} - 1$ and $\beta_0 = \frac{\tilde{\beta}}{n+1}$ (in addition to the cited paper [40], this procedure can also be seen in Ref. [41]). When $n \to \infty$ ($q \to 1$), the MD equation (13) is recovered.

On the other hand, if $E = v^2/2$, $c = \frac{n+1}{2}$, and $\beta_0 = b(c - 1/2)$ in Eq. (15), we have $B(E) = (1 + bE)^{-c}$ as is shown by the authors of Ref. [4], which is equivalent to $\exp(-c \ln(1 + bE))$. Just as they did, we too can take from Eq. (15) an expansion, in such a way that we are left with the un-normalized CD function

$$p_c(v) = e^{-\frac{1}{2}\beta_0 v^2} \left(1 + \frac{1}{8}\sigma^2 \beta_0^2 v^4\right), \tag{16}$$

with σ^2 variance of $f(\beta)$, as is shown in Ref. [42]. So, from these results the CTD function can arise, obtaining

$$p_{CT}(v) = C_{q,\alpha} \left(1 + \alpha \beta_0^2 v^4\right) \left(1 + (q-1)\frac{\beta_0 v^2}{2}\right)^{-\frac{1}{q-1}}, \tag{17}$$

where $C_{q,\alpha}$ is the constant of normalization.

IV. RESULTS

A. Molecular dynamics simulation

Atypical distribution of velocities in QSSs of the d-HMF model can be seen when the molecular dynamics simulation is performed. We take a symplectic integrator and water-bag initial conditions applied to $N = 16\,384$ identical coupled particles (mass equal to 1 and energy $U = 1.38$). The graphical results presented later in this section are derived from a set consisting of the average of 100 independent simulations performed for that particular energy level. This method based on averaging over multiple similar realizations not only provides a more robust and reliable representation of the data, but also mitigates the influence of stochastic fluctuations inherent in the underlying process. In this way, a more complete and precise view of the trends and behaviors observed in the study is achieved.

B. Application of the Cairns-Tsallis distribution

Let us start by observing the time evolution plots of the average kinetic energy and magnetization, which have been shown by different authors to highlight peculiar characteristics of HMF and d-HMF models. We can readily observe in Fig. 5 two quasistationary states experienced by the system, which are reflected in transitions both in the average kinetic energy and the magnetization. The first of them, QSS-1, occurs at the beginning of the simulation, extending up to roughly $t = 1000$, while QSS-2 persists approximately between $t = 30\,000$ and $t = 900\,000$. After this, a transition
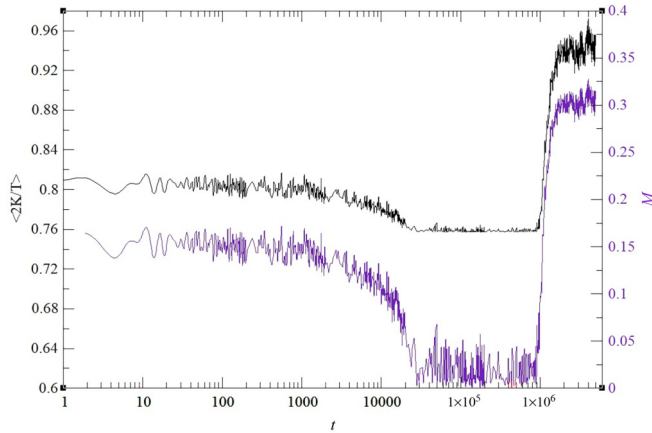
FIG. 5. Average kinetic energy $\langle 2K/N \rangle$ and magnetization M evolution for $N = 16\,384$, showing two quasistationary states appearing during the d-HMF simulation.

to the equilibrium state occurs. We note that the QSSs can be observed in different thermodynamic quantities. These quantities exhibit the same behavior during the transition to equilibrium. We can observe the emergence of plateaus for both QSSs.

In the following we analyze fit parameters q and α obtained with the CTD function, to check if they show characteristic values for each quasistationary state, in addition to the already known values for the equilibrium state, namely, $q \to 1$ and $\alpha \to 0$. We found by proceeding that the obtained fit curves (and therefore the fit parameters) for the corresponding velocity distributions show different dynamic behaviors during the QSS-1 and QSS-2 periods. It is possible to see in Fig. 6, as an example, that the fit curves show more pronounced "shoulders" during QSS-1 than during QSS-2, represented by $t = 100$ and $t = 600$ in the first case and by $t = 500\,000$ and $t = 800\,000$ in the second one. Such a feature allows us to characterize the system with clear differences in the corresponding fit parameters. To better visualize the effect on the fit values of the q and α parameters, we present Figs. 7 and 8, obtained at 60 time points arbitrarily chosen throughout the entire simulation.
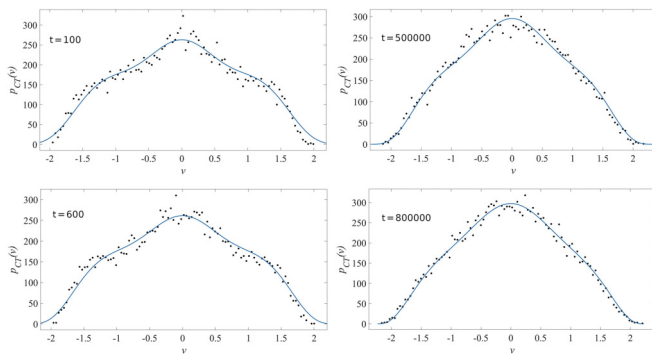

FIG. 6. Four representative instants of time in the d-HMF simulation, $t = 100$ and $t = 600$ (both in QSS-1) and $t = 500\,000$ and $t = 800\,000$ (both in QSS-2), showing the respective fit curves obtained with the CTD function.
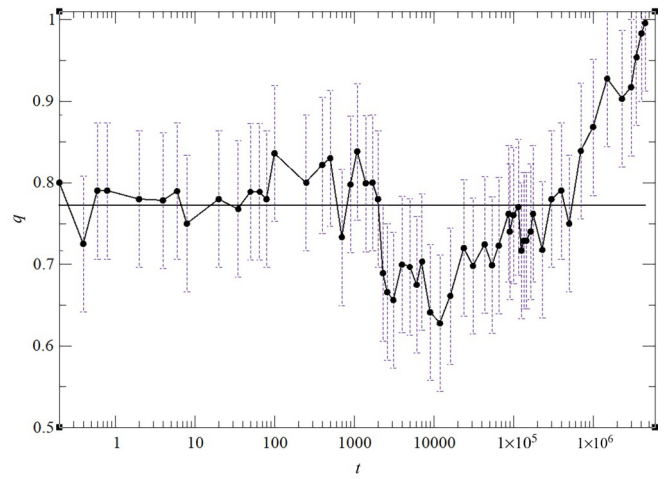

FIG. 7. Evolution of the fit parameter q, the values of which were obtained in 60 instants of time during the d-HMF simulation (for reference, we draw a baseline with the average of the data set).

V. FINAL REMARKS

As seen in Sec. IV, the time evolution of the average kinetic energy and magnetization, obtained with data outputs from the d-HMF simulation, has shown two quasistationary states, QSS-1 and QSS-2 (different from each other), and a final evolution towards the equilibrium state (Fig. 5). The nature of both QSSs involved in the dynamics towards equilibrium is shown in Fig. 2. QSS-1 is depicted in Figs. 2(a) and 2(b). It can be observed how this state still has a strong correlation with the initial conditions, where most of the dipoles are oriented in a parallel manner, i.e., $\theta_i \approx 0$. QSS-2 is illustrated in Fig. 2(c); here the dipoles describe a uniform distribution in orientations, implying that the restoring forces are close to zero, thus keeping the system in a quasiequilibrium with zero magnetization. Subsequently, the system evolves towards equilibrium, where the momentum distribution becomes Gaussian. Consistent with the above, we also found
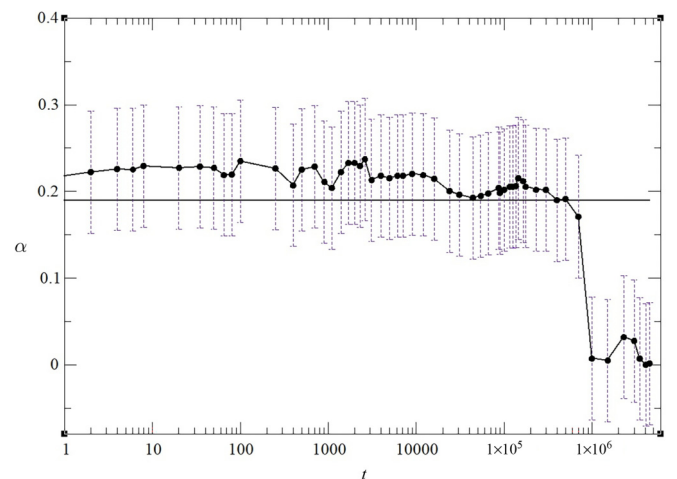

FIG. 8. Evolution of the fit parameter α, the values of which were obtained in 60 instants of time during the d-HMF simulation (for reference, we draw a baseline with the average of the data set).

that both states, QSS-1 and QSS-2, are also reflected through the CTD function when it is fitted in different instants of time to the corresponding velocity distribution. Values of the q and α parameters reveal the presence of both quasistationary states, generating fit curves with a greater widening of shoulders for QSS-1 than for QSS-2 (Fig. 6). The emergence of shoulders in the momentum distribution of QSS-1 is possibly because the particles remain strongly tied to the initial conditions, which can be understood as a clustering phenomenon. Those particular curve fittings achieved by the CTD function are impossible to achieve with many other models found in the literature, as can be seen in Sec. II, where a Tsallis-like function, which is a solution of the Vlasov equation, was applied to an instant of time of the stationary state during the corresponding simulation.

We see that fit values for α tend to decrease very slightly when the simulated system remains in QSS-2, unlike what is observed in QSS-1. However, we can see a particularity that is worth mentioning, which refers to the upper limit that seems to exist for the α values. We can see in Fig. 8 that in QSS-1 and QSS-2, fit values for α are very close to 0.250 (the closest one is $\alpha_{max} = 0.237$, which occurs at $t = 2600$) and, on the other hand, $\alpha \to 0$ when the system tends to equilibrium ($\alpha_{min} = 9 \times 10^{-9}$ at $t = 5 \times 10^6$). The above makes sense inside of a plasma context, due to the fact that the upper limit $\alpha = 0.25$ has already been found through the normalized electron density, which was obtained by integrating the Cairns function (details can be reviewed in Ref. [43]). Many authors estimate that for $\alpha < 0.25$ the Cairns distribution is properly defined (e.g., it was found in Ref. [44] that $0.155 < \alpha < 0.25$ are relevant values to consider). Since the nonthermality parameter α is a deviation measure from a Maxwellian distribution (where $\alpha = 0$), α values closer to 0.25 imply that the plasma system is more likely to exhibit instabilities and turbulence, as well as being affected by nonthermal processes.

On the other hand, the nonextensivity q parameter is further from $q = 1$ in QSS-2 than in QSS-1. Then, it seems that in QSS-2 we have a system subjected to stronger long-range interactions while transiting through the nonequilibrium state. In addition, by checking that $q \to 1$ and $\alpha \to 0$ in Figs. 7 and 8, the equilibrium state can be clearly observed from $t = 10^6$, as expected. Here we also have some relevant additional remarks to make, since of the total of 60 fit values obtained for parameter q during the performed simulation (shown in Fig. 7) we find that all the fit values fall into the interval [0.628,0.996]. The above makes sense again when we return to the plasma viewpoint. For example, properties of the CTD function were investigated in the context of ion acoustic soliton behavior in plasmas with excess superthermal particles [31], showing that outside of $0.6 < q \leqslant 1$ the CTD function may present drawbacks associated with the distribution itself or the respective normalization (and these are the reasons why the authors of Ref. [31] warned us about its severely restricted applicability).

In summary, this research offers a comprehensive and improved description of the QSSs in the d-HMF model. We have obtained a satisfactory depiction of these states by means of the Cairns-Tsallis distribution, because the velocity distribution obtained from the d-HMF model provides us fit values for the q and α parameters that are *ad hoc* with values observed in applications of the CTD function to nonthermal plasmas. Application of the CTD function in long-range interacting systems could be of great interest. Hence an approach such as the one presented in this paper could be explored in other systems, such as the HMF model, self-gravitating systems, and the ring model, among others, that could be relevant in future works.

[1] V. Vasyliunas, A survey of low-energy electrons in the evening sector of the magnetosphere with OGO 1 and OGO 3, J. Geophys. Res. **73**, 2839 (1968).

[2] D. Lynden-Bell, Statistical mechanics of violent relaxation in stellar systems, Mon. Not. R. Astron. Soc. **136**, 101 (1967).

[3] C. Tsallis, Possible generalization of Boltzmann–Gibbs statistics, J. Stat. Phys. **52**, 479 (1988).

[4] C. Beck and E. Cohen, Superstatistic, Phys. A (Amsterdam) **322**, 267 (2003).

[5] E. Jaynes, The minimum entropy production principle, Annu. Rev. Phys. Chem. **31**, 579 (1980).

[6] Y. Levin, R. Pakter, F. Rizzato, T. Teles, and F. Benetti, Nonequilibrium statistical mechanics of systems with long-range interactions, Phys. Rep. **535**, 1 (2014).

[7] F. D. Nobre, E. M. F. Curado, A. M. C. Souza, and R. F. S. Andrade, Consistent thermodynamic framework for interacting particles by neglecting thermal noise, Phys. Rev. E **91**, 022135 (2015).

[8] M. S. Ribeiro, G. A. Casas, and F. D. Nobre, Second law and entropy production in a nonextensive system, Phys. Rev. E **91**, 012140 (2015).

[9] M. Ribeiro, F. Nobre, and E. Curado, Time evolution of interacting vortices under overdamped motion, Phys. Rev. E **85**, 021146 (2012).

[10] A. R. Plastino, E. Curado, F. Nobre, and C. Tsallis, From the nonlinear Fokker-Planck equation to the Vlasov description and back: Confined interacting particles with drag, Phys. Rev. E **97**, 022120 (2018).

[11] B. Atenas and S. Curilef, Dynamics and thermodynamics of systems with long-range dipole-type interactions, Phys. Rev. E **95**, 022110 (2017).

[12] B. Atenas, Dynamics and thermodynamics of the mean field d-HMF model out-of-equilibrium, M.S. thesis, Universidad Católica del Norte, Chile, 2021.

[13] B. Atenas and S. Curilef, Dynamics of the d-HMF model: Sensitive dependence on size and initial conditions, J. Phys.: Conf. Ser. **1043**, 012009 (2018).

[14] B. Atenas and S. Curilef, A solvable problem in statistical mechanics: The dipole-type Hamiltonian mean field model, Ann. Phys. (Amsterdam) **409**, 167926 (2019).

[15] B. Atenas and S. Curilef, A statistical description for the quasi-stationary-states of the dipole-type Hamiltonian mean field

field model based on a family of Vlasov solutions, Phys. A (Amsterdam) **568**, 125722 (2021).

[16] A. Pluchino, V. Latora, and A. Rapisarda, Dynamics and thermodynamics of a model with long-range interactions, Continuum Mech. Thermodyn. **16**, 245 (2004).

[17] A. Pluchino, A. Rapisarda, and C. Tsallis, A closer look at the indications of q-generalized central limit theorem behavior in quasi-stationary states of the HMF model, Phys. A (Amsterdam) **387**, 3121 (2008).

[18] R. Moreira, B. Atenas, J. A. Navarro, and S. Curilef, On the trajectories of the quasi-stationary states in the d-HMF model, AIP Conf. Proc. **2731**, 030005 (2023).

[19] D. Summers and R. Thorne, The modified plasma dispersion function, Phys. Fluids B **3**, 1835 (1991).

[20] M. Leubner, A nonextensive entropy approach to kappa-distributions, Astrophys. Space Sci. **282**, 573 (2002).

[21] G. Livadiotis and D. McComas, Beyond kappa distributions: Exploiting Tsallis statistical mechanics in space plasmas, J. Geophys. Res. **114**, A11105 (2009).

[22] G. Livadiotis, Kappa and q indices: Dependence on the degrees of freedom, Entropy **17**, 2062 (2015).

[23] R. Cairns, A. Mamum, R. Bingham, R. Boström, R. Dendy, C. Nairn, and P. Shukla, Electrostatic solitary structures in non-thermal plasmas, Geophys. Res. Lett. **22**, 2709 (1995).

[24] B. Zenteno-Quinteros, A. F. Viñas, and P. S. Moya, Skew-kappa distribution functions and Whistler heat flux instability in the solar wind: The core-Strahlo model, Astrophys. J. **923**, 180 (2021).

[25] M. Qureshi, H. Shah, G. Murtaza, S. Schwartz, and F. Mahmood, Parallel propagating electromagnetic modes with the generalized (r, q) distribution function, Phys. Plasmas **11**, 3819 (2004).

[26] M. Tribeche, R. Amour, and P. K. Shukla, Ion acoustic solitary waves in a plasma with nonthermal electrons featuring Tsallis distribution, Phys. Rev. E **85**, 037401 (2012).

[27] J. A. S. Lima, R. Silva, and J. Santos, Plasma oscillations and nonextensive statistics, Phys. Rev. E **61**, 3260 (2000).

[28] M. Ghorbanalilu, E. Abdollahzadeh, and S. Rahbari, Particle-in-cell simulation of two stream instability in the non-extensive statistics, Laser Part. Beams **32**, 399 (2014).

[29] A. Ur-Rehman and J. K. Lee, Electron acoustic waves in a plasma with a q-nonextensive distribution of electrons, Phys. Plasmas **25**, 022107 (2018).

[30] R. Amour and M. T. P. Shukla, Electron acoustic solitary waves in a plasma with nonthermal electrons featuring Tsallis distribution, Astrophys. Space Sci. **338**, 287 (2012).

[31] G. Williams, I. Kourakis, F. Verheest, and M. A. Hellberg, Re-examining the Cairns-Tsallis model for ion acoustic solitons, Phys. Rev. E **88**, 023103 (2013).

[32] S. Bansal and M. Aggarwal, Non-planar electron-acoustic waves with hybrid Cairns–Tsallis distribution, Pramana - J. Phys. **92**, 49 (2019).

[33] P. Bala, A. Kaur, and K. Kaur, Arbitrary amplitude electron-acoustic solitons and double layers with Cairns–Tsallis-distributed hot electrons, Pramana - J. Phys. **95**, 20 (2021).

[34] A. A. Abid, S. L. Y. M. Z. Khan, H. Terças, and S. Mahmood, Dust charging processes with a Cairns-Tsallis distribution function with negative ions, Phys. Plasmas **23**, 013706 (2016).

[35] M. Farooq, M. Ahmad, and Q. Jan, Polarization force in an opposite polarity dusty plasma with hybrid Cairns–Tsallis distributed electrons, Contrib. Plasma Phys. **61**, e202000170 (2021).

[36] S. Davis, G. Avaria, B. Bora, J. Jain, J. Moreno, C. Pavez, and L. Soto, Single-particle velocity distributions of collisionless, steady-state plasmas must follow superstatistics, Phys. Rev. E **100**, 023205 (2019).

[37] E. Sanchez, M. Gonzalez-Navarrete, and C. Caamaño-Carrillo, Bivariate superstatistics: An application to statistical plasma physics, Eur. Phys. J. B **94**, 55 (2021).

[38] S. Khalfaoui, S. Dilmi, and A. Boumali, On the calculation of superstatistics ionization rates of neutral Hélium, Phys. A (Amsterdam) **596**, 127193 (2022).

[39] S. Dilmi, F. Khalfaoui, and A. Boumali, The effects of super-statistics properties on hot plasma, Eng. Technol. Appl. Sci. Res. **12**, 9342 (2022).

[40] K. Ourabah and L. A. Gougam, Nonthermal and suprathermal distributions as a consequence of superstatistics, Phys. Rev. E **91**, 012133 (2015).

[41] P. Yoon, Non-equilibrium statistical mechanical approach to the formation of non-Maxwellian electron distribution in space, Eur. Phys. J. Special Topics **229**, 819 (2020).

[42] K. Ourabah, Demystifying the success of empirical distributions in space plasmas, Phys. Rev. Res. **2**, 023121 (2020).

[43] F. Verheest and S. R. Pillay, Large amplitude dust-acoustic solitary waves and double layers in nonthermal plasmas, Phys. Plasmas **15**, 013703 (2008).

[44] K. Annou, D. Bara, and D. B.-Doumaz, Cairns-Gurevich equation for soliton in plasma expansion into vacuum, J. Plasma Phys. **81**, 905810318 (2015).